Inorganica Chimica Acta 503 (2020) 119375

Contents lists available at ScienceDirect

Inorganica Chimica Acta

journal homepage: www.elsevier.com/locate/ica

Research paper

Exploring six-coordinate germanium(IV)-diketonate complexes as anticancer agents

Randall T. Mertens, Sean Parkin, Samuel G. Awuah*

Department of Chemistry, College of Arts and Sciences, University of Kentucky, 505 Rose Street, Lexington, KY 40506-0055, USA

ARTICLE INFO

Keywords:
Germanium
Anticancer
Metalloid
Cytotoxicity
Drug discovery
Resistance

ABSTRACT

Cancer remains one of the leading causes of death worldwide and despite several attempts using chemotherapy to combat the deadly disease, toxic side effects and drug resistance temper efficacy [1]. Thus, drugs with potentially new mechanisms and lower toxicity to normal cells are needed. Metalloids such as arsenic compounds have been clinically beneficial in fighting cancer, but germanium is yet to gain such prominence [2,3]. We report the synthesis of four octahedral germanium(IV) complexes bearing acetylacetonato ligand, $[Ge^{IV}(acac)_3)]^+$, with different anions (**3** – **6**) using a streamlined synthetic approach. The compounds were structurally and electrochemically characterized using NMR, MS, X-ray crystallography, and cyclic voltammetry. The cyclic voltammogram of **3–5** revealed distinct irreversible peaks in the range of −0.9 to −1.9 V, corresponding to Ge(IV)/Ge(II) or Ge(II)/Ge(0) couple in DMSO. We explored the anticancer activity of the complexes against a panel of cancer cell lines with IC_{50} values in the sub-micromolar range (9–15 μM). The compounds display ~3-fold selectivity in cancer cells over normal epithelial cells. In addition to the promising anticancer activity, the compounds display high complex stability in biological media, induces G1 arrest, reactive oxygen stress (ROS) accumulation, and mitochondria membrane depolarization in cancer cells. Furthermore, the compounds induce significant apoptosis.

1. Introduction

Metallodrug discovery holds an important place in the quest for effective chemotherapeutic agents in the fight against cancer [1–4]. Cisplatin, carboplatin, and oxaliplatin are platinum-based drugs approved by the FDA that are first-line therapeutics for several cancer types including, ovarian, testicular, endometrial, lung, and colon cancers [5–7]. Despite transformational outcomes of these agents, drawbacks including innate and acquired resistance, and toxic side effects often precipitate tumor recurrence and even death [8]. Research efforts toward the development of efficacious inorganic agents using other transition metals or metalloids is on the rise. Ideal compounds will possess potent activity against cancer cells while sparing normal cells and induce cancer-specific cell death through differentiated mechanisms from platinum agents. Thus, the use of metalloids with characteristically different reactivity and electronic properties could be clinically relevant. Metalloids on the periodic table consist of boron, silicon, germanium, arsenic, antimony, tellurium, and polonium. The discovery of metalloid-based drugs has shown significant promise in the clinic, exemplified in Velcade (bortezomib), which is a proteasome inhibitor for the treatment of multiple myeloma; arsenic trioxide for acute promyelocytic leukaemia therapy; and high-valent antimony that treats leishmaniasis (Fig. 1) [9–12]. Whereas impressive scientific advancements have been made with boron, arsenic, and antimony in metalloid drug discovery, germanium remains relatively underexplored [13,14].

Germanium exists in trace amounts in plants and other living matter [15–17]. The rather popular germanium sesquioxide is used as a dietary supplement for its antioxidative properties [14,18,19]. Carboxyethyl germanium sesquioxide is found in the Reishi mushroom and Ginseng. Biomedical applications of germanium oxide (GeO_2) and germanium nanoparticles as radiosensitizers have been reported [20–23]. The organometallic germanium complex, spirogermanium was tested in phase II clinical trials against a number of solid tumours and malignant lymphomas [24–27]. The antineoplastic activity of spirogermanium was tempered by acute neurotoxicity. Furthermore, Ge(IV) polyphenols possess promising anticancer effects [13]. A more systematic investigation of bioactive germanium compounds will unravel pharmacologically active agents towards indications such as cancer.

Work in our laboratory has focused on understanding and developing transition metal and metalloid compounds as anticancer agents. The previously outlined success with metalloids in various therapies and the use of metalloid ligands in our laboratory's recent research

* Corresponding author.
E-mail address: awuah@uky.edu (S.G. Awuah).

https://doi.org/10.1016/j.ica.2019.119375
Received 7 November 2019; Received in revised form 11 December 2019; Accepted 12 December 2019
Available online 19 December 2019

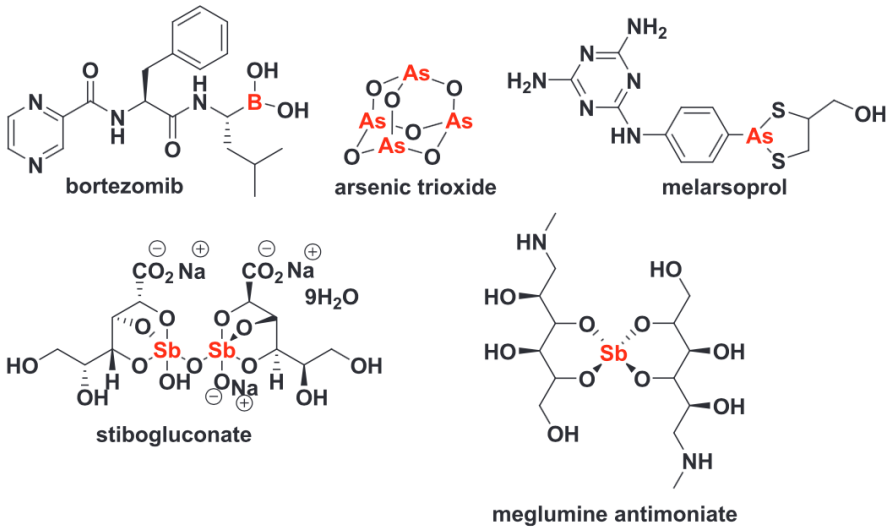

Fig. 1. Structure of approved metalloid-containing drugs for different disease indications.

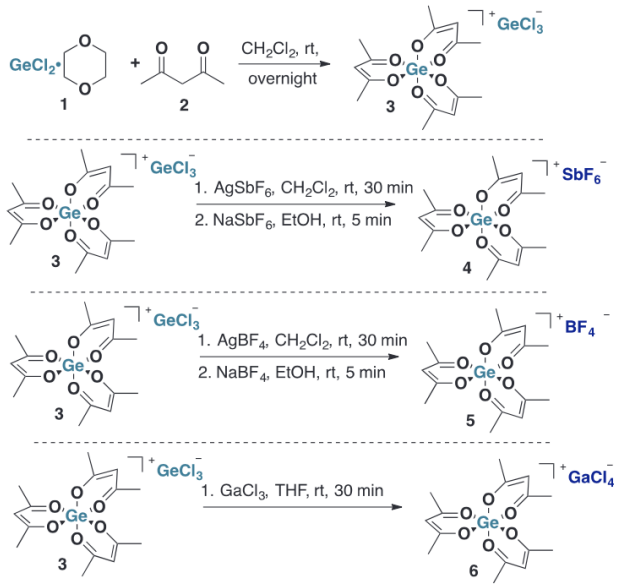

Scheme 1. Synthetic schemes showing the preparation of the Ge complexes **3 – 6**.

efforts led us to consider the use of germanium as a potential therapeutic. In this work, we used acetylacetonato, which is a commonly used ligand in the synthesis of metal triads, to synthesize octahedral germanium salts $[Ge(acac)_3)]^+$ of different anions including a mixed valent Ge(IV) cationic complex with a Ge(II) anionic counterion [28]. Metalloid triads are quite rare in the literature with two formal reports of six-coordinate β-diketonate ($acac^-$) Ge(IV) complexes of the type: $[Ge(acac)_3][FeCl_4]$ and $[Ge(acac)_2Cl_2]$ [29,30]. It must be noted that the ($acac^-$) ligand has been employed as a suitable ligand for third-row transition metal complexes including $Ir(acac)_3$, $Ru(acac)_3$, and $Pt(acac)_2$, and they possess antitumor activity [31,32]. Herein, we present the structure and electrochemical characterization of novel Ge(IV) β-diketonates, **3–6** (Scheme 1). Following the solution studies of these agents the anticancer activity of **3–6** was assessed against cisplatin sensitive and refractory cell lines [33]. We also present the cell cycle response to compound **3** in order to gain insight into its potential mechanism of action. The compounds induce apoptosis potentially through ROS accumulation and mitochondrial membrane depolarization in cancer cells.

2. Results and discussion

2.1. Chemical synthesis and characterization

Inspired by the use of Ge(IV) coordination /organometalloid agents as antioxidants or of therapeutic benefit, we rationalized that the use of β-diketonates and the influence of distinct anions will provide a rapid platform to explore the anticancer potential of germanium. The new class of Ge(IV)-(acac) complexes were synthesized from $Ge(II)Cl_2$ dioxane and acetylacetone at room temperature. The ($acac^-$) is a bidentate ligand that displaces the Cl ligands and the loosely bound dioxane adduct to obtain the six-coordinate β-diketonate complex. This deviates from reported protocols that react $[Fe(acac)_3]^+$ and group IV tetrachlorides (MCl_4) to make rearranged products, $[M(acac)_3][FeCl_4]$ [29,34–37]. Our synthetic method gives rise to a novel mixed valence Ge complex of the type, $[Ge(IV)(acac)_3][Ge(II)Cl_3]$ (Scheme. 1). Additionally, the synthetic approach is streamlined to access different complexes with varying anions, including $[Ge(acac)_3][SbF_6]$ (**4**) and $[Ge(acac)_3][BF_4]$ (**5**), and the unstable $[Ge(acac)_3][GaCl_4]$ (**6**), which were synthesized by reacting **3** with different silver salts, leading to substitution of the $GeCl_3^-$ anion with SbF_6^- (**4**) or BF_4^- (**5**) and $GaCl_4^-$ to obtain **6**. The structures of these complexes are supported by single X-ray crystallography, multinuclear NMR spectroscopy, and liquid chromatography mass spectrometry (LC-MS). The purity of the complexes was further ascertained by elemental analysis and HPLC of > 97%.

2.2. X-ray crystallography

Colourless single crystals of complexes **3, 4, 5** were grown from slow evaporation of a dichloromethane solution. Crystals of **6** were grown from slow evaporation of a THF solution under a counter flow of N_2 on the Schlenk line. Single X-ray investigations of the newly synthesized complexes show average bond lengths of Ge–O = 1.863 Å to 1.872 Å within the coordination sphere of the cation. The observed bond lengths are longer than the observed Ge = O bonds in GeO_2 (1.737 to 1.741 Å) [38]. Classical examples of organogermane compounds exhibit similar shorter Ge-O bond lengths, e.g. $(PhCH_2)GeOGe(CH_2Ph)_3$ and $Ph_3SiOGePh_3$, distances of 1.73 Å [39,40] and 1.70 Å [39,41] respectively. Longer Ge-O bonds are typically found in high-valent organogermanium compounds such as $Ge_2O_2C_{40}H_{52}$ with a Ge-O bond length of 1.857 Å [42]. Due to the high-valent nature of these tris-acetylacetonato complexes and back donation of electrons from

Table 1
X-ray crystal structure data with solution and refinement parameters for compounds **3 – 6**.

X-ray Structural Data and Crystal Refinement				
Empirical Formula	**3** $C_{15}H_{21}Ge_2O_6Cl_3$	**4** $C_{15}H_{21}GeO_6SbF_6$	**5** $C_{15}H_{21}GeO_6BF_4$	**6** $C_{15}H_{21}GeO_6GaCl_4$
Molecular Weight (g/mol)	548.85	605.66	456.72	581.43
Temperature (K)	90.0(2)	90.0(2)	90.0(2)	90.0(2)
X-ray Radiation (Å)	Mo Kα (0.71073 Å)	Mo Kα (0.71073 Å)	Mo Kα (0.71073 Å)	Mo Kα (0.71073 Å)
Crystal System, Space Group	Monoclinic, I2/a	Trigonal, *P*-31*c*	Monoclinic, *C*2/*c*	Monoclinic, $P2_1/n$
Unit Cell Dimensions (A), (°)	a = 23.1901(7) A alpha = 90 b = 7.6888(2) A beta = 104.391(2) c = 25.8892(7) A gamma = 90	a = 10.5197(2) A alpha = 90 b = 10.5197(2) A beta = 90 c = 10.7111(2) A gamma = 120	a = 34.3684(10)Å alpha = 90 b = 12.5546(4) Å beta = 110.370(1) c = 13.9568(3) Å gamma = 90	a = 7.5483(1) A alpha = 90 b = 19.8167(4) A beta = 99.488(1) c = 15.2969(3) A gamma = 90
Volume	5645.5(3) $Å^3$	1026.53(4) $Å^3$	5645.5(3) $Å^3$	2256.85(7) $Å^3$
Z	8	2	12	4
Absorption Coefficient	3.073 mm^{-1}	2.862 mm^{-1}	1.695 mm^{-1}	3.026 mm^{-1}
F(0 0 0)	2192	592	2784	1160
Crystal Size (mm)	0.230 × 0.180 × 0.080	0.200 × 0.170 × 0.140	0.200 × 0.200 × 0.080	0.120 × 0.050 × 0.060
Theta Range	2.719 to 27.448	2.935 to 27.457	2.478 to 27.510	2.459 to 27.491
Completeness to Theta = 25.242	99.90%	99.50%	99.90%	100.00%
S (goodness-of-fit)	1.116	1.123	1.02	1.059
Final R indices [I > 2sigma(I)]	R1 = 0.0328, w*R*2 = 0.0874	R1 = 0.0132, w*R*2 = 0.0341	R1 = 0.0241, w*R*2 = 0.0544	R1 = 0.0270, w*R*2 = 0.0506

germanium to resonance stabilized ligand, the observed lengths are similar to other Ge(IV) compounds previously reported in the literature [39]. The observed bond lengths of C—O and C—C for the acetylacetonato ligand are 1.292 to 1.302 Å and 1.386 to 1.387 Å respectively. Single C—O bond lengths have a distance of 1.43 Å while C═O bonds have a distance of 1.20 Å [43]. The observed C—O bond lengths found in compounds **3 – 6** fall in between a C═O and C—O bond due to the pi-system of the acetylacetonato ligand. Similarly, the C—C bond lengths in compounds **3 – 6** are in between the length of a C═C and C—C bond (1.34 Å and 1.54 Å) [43] which is also due to the resonance of the acetylacetonato ligand. The bond lengths and angles of complexes **3–6** compare with the interatomic parameters observed for similar structures of Ge(IV) complexes such as Ge(IV)-polyphenols or [Ge $(acac)_2Cl_2$)] [13,30].

All compounds crystallize out in space groups with an inversion symmetry operation (Table 1). Due to the octahedral geometry and D_3 point group of the complexes, **3–6** exist as a 50:50 enantiomeric mixture between the delta (Δ) and lambda (Λ) isomers. Compound **4** crystallizes with a high symmetry trigonal space group, group $P\bar{3}1c$. The $[Ge(acac)_3]^+$ cation sits on a $\bar{3}$ axis of the space group $P\bar{3}1c$ while the SbF_6^- anion sits on a site of 32 point symmetry (Wyckoff site c). Compound **5** crystallizes out with 1.5 cations and 1.5 anions in the asymmetric unit; therefore two whole molecules are projected in the diagram in Fig. 2.

2.3. Electrochemistry

We characterized the electrochemical behaviour of **3–5** by cyclic voltammetry in anhydrous DMSO at concentrations of 10 mM with 0.1 M NH_4PF_6 as the supporting electrolyte (Fig. 3). The condition used for the study are a scan rate of 100 mV/s, referenced to Ag/AgCl and positioned to Fc/Fc + couple as the internal standard. Full cyclic voltammograms of **3–5** and respective controls are displayed in the supporting information (Figs. S15–S17). The cyclic voltammogram of **3–5** revealed a distinct irreversible peak (A) [**3** = −1.2 V, **4** = −1.3 V, and **5** = −0.9]. We attribute this reduction peak to a Ge^{IV}/Ge^{II} couple. For compounds **3** and **5**, a second irreversible peak (B) was observed [**3** = −1.9 V, and **5** = −1.9 V] consistent with a Ge^{II}/Ge^0 couple. Compound **3** had an additional irreversible wave (C) [−1.5 V], which was assigned to the Ge^{II}/Ge^0 couple associated with the low-valent $GeCl_3^-$ counter-anion. An oxidation wave (D) was observed in complex **3** and **4** (Table 2). This is likely oxidation of the acetylacetonato ligand. The two-electron Ge^{IV}/Ge^{II} reduction potential is −1.37 V and that of Ge^{II}/Ge^0 is −1.07 V. The observed reduction potentials for our complexes are consistent with other reported Ge(IV) complexes such as halogermanate(IV) compounds.[44] It is important to note that the nature of the counterion affects electrochemical behaviour, in that, while **3** and **5** display two distinct 2-electron reduction events, compound **4** bearing the SbF_6^- anion shows only one 2-electron reduction event. This suggests that compound **4** undergoes only Ge^{IV}/Ge^{II} reduction with no Ge^{II}/Ge^0. Additionally, complex **3,** possesses the $GeCl_3^-$ anion displays redox activity, and could have implications for the overall stability of the complex. Stability for inorganic complexes is an essential property for therapeutic development and as shown with these complexes, the different anions change the redox behaviour of the complexes with potential implications on compound stability. For example, compound **6**, with a $GaCl_4^-$ anion is not stable in air and highly susceptible to sublimation. Taken together, we offer insights into the electrochemical behaviour of Ge(IV) complexes and how the counter anions impart redox activity and stability.

2.4. Solution chemistry

Complexes **3–5** display good solubility in DMSO with distinct UV–Vis peaks at 300 nm and 570 nm. This could be attributed to variations of ligand-to-metalloid or metalloid-to-ligand charge transfer (Fig. 4). We exploited the UV-vis features in solution to examine the stability of the complexes under physiological conditions. In Dubelcco's Eagle Modified Medium (DMEM), the peak at 300 nm reduced by 30% in absorption units for **3**, while that of 570 nm remained unchanged over a period of 48 h. Note that DMEM contains numerous biological reductants, hence our observation is significant, given that the complexes show minimal degradation in solution over 48 h, indicative of good stability. The UV-vis profile for complex **4** show no alteration in peaks throughout the time-course of the study. Evidence of anion effects are observed as SbF_6^- demonstrates superior stability over complexes with $GeCl_3^-$ or BF_4^- counteranion.

2.5. Stability Studies: Reactivity with L-Glutathione (GSH) and N-Acetyl cysteine (NAC)

Solution stability of complexes is critical when developing new therapeutics. Transition metal complexes such as gold(III) dithiocarbamates are easily reduced under biological conditions by

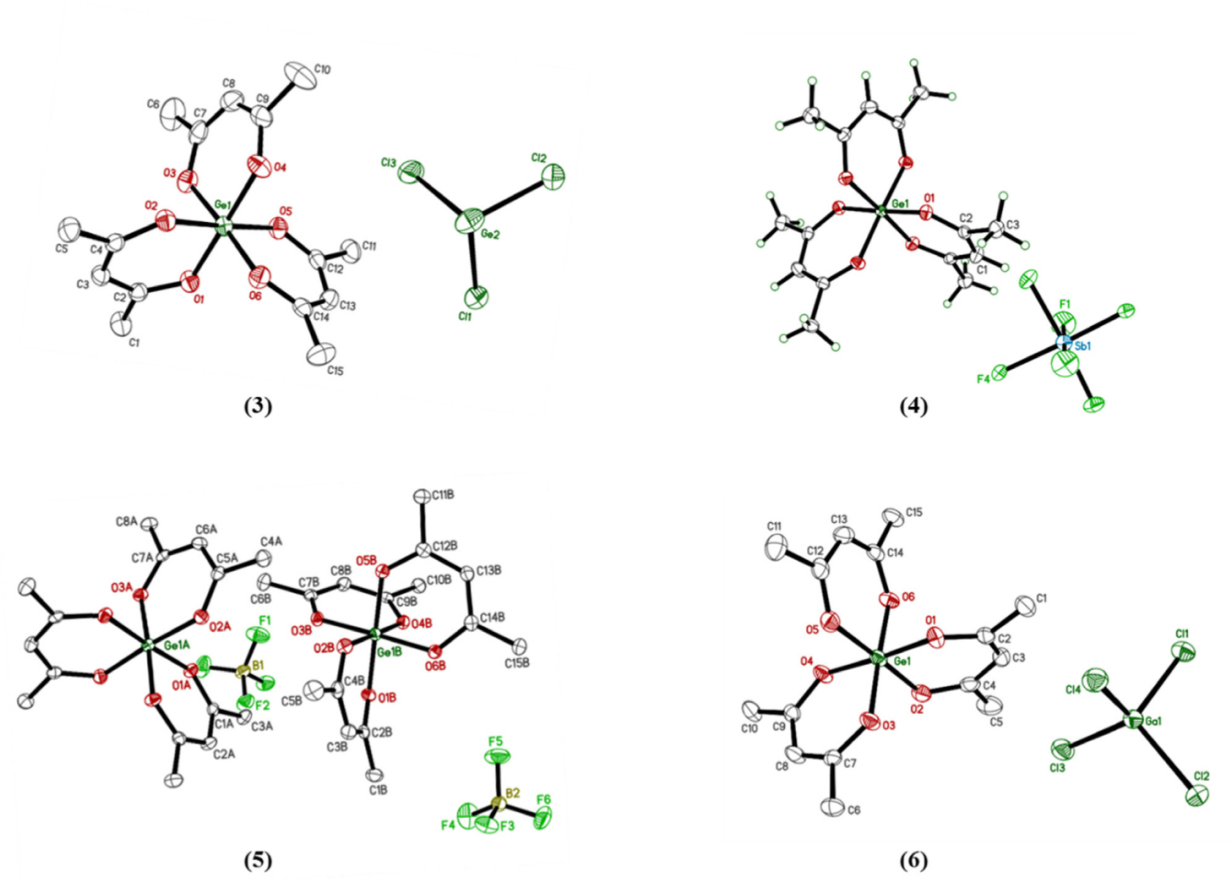

Fig. 2. X-ray crystal structures of compounds **3**, **4**, **5**, and **6**. Ellipsoids are drawn at 50% probability level. Hydrogen atoms bound to carbon atoms are omitted for clarity. In **(5)**, the 'A' molecule sits on a crystallographic 2-fold axis.

nucleophilic biomolecules such as L-glutathione [45,46]. Although these complexes possess high *in vitro* activity, their lack of stability makes them less appealing than other transition metal complexes. Transition metal complexes are not the only type of complexes that suffer from a decrease in activity when exposed to elevated concentrations of GSH. Bortezomib, the aforementioned FDA approved example of a metalloid based drug, was shown to have decreased activity in multiple myeloma cells when exposed to excess GSH levels [47]. These studies are clearly indicative that compound stability towards reducing biomolecules play a pivotal role in the development of effective therapeutics. To evaluate the stability of our complexes, UV–vis spectrometry was employed to determine the reactivity profile of **3** towards both the tri-peptide, GSH and the nucleophilic amino acid, NAC. The estimated intracellular levels of GSH are estimated to be ~10 mM [48,49]. We exposed complex **3** to 5 mM of GSH (Fig. 5A) and 5 mM NAC (Fig. 5B) in a 1:10 ratio over a period of 24 h to assess the stability of **3** towards these biomolecules.

After 24 h exposure of **3** with both GSH and NAC in a 1:10 M ratio, no significant change could be observed. The absorbance attributed to **3** at 300 nm was minimally altered with a slight decrease in overall absorbance; however, this decrease is attributed to the natural decay of absorbance in DMEM over time as previously shown in Fig. 4. The solution studies suggest that the compounds are not deactivated by biological nucleophiles and may not bind other biological nucleophiles such as DNA bases. It is likely that these agents generate ROS as demonstrated in ROS accumulation studies and mitochondria membrane depolarization studies, *vide infra*.

2.6. Cell viability

Using MTT assays, we evaluated the anticancer activity of **3–5** in human cancer cell lines, including ovarian adenocarcinoma cell line, A2780; triple negative breast cancer (TNBC) cell lines, MDA-MB-231 and MDA-MB-175; and the lung cancer cell line, H460. It became evident that the cytotoxicity of **3–5** was more effective against cisplatin-resistant cancer cells, MDA-MB-231 and MDA-MB-175 with IC_{50} of 10 μM and 14 μM respectively in comparison to ~4.7–180 μM for cisplatin in the same cell lines as summarized in Table 3. Despite the modest cytotoxicity of these agents, it is likely that further ligand optimization will improve their potency to exploit vulnerabilities in TNBCs, which have proven refractory to platinum therapy [50–52]. In lieu of the modest toxicity towards TNBC's, complexes **3–5** exhibited less toxicity towards the healthy cell line, MRC5. The IC_{50} values of compounds **3–5** are ~3 times greater than that reported for cisplatin in MRC5 normal cells. This gives promise moving forward as preliminary data suggests these complexes possess some selectivity towards cancerous cell lines versus healthy cell lines.

2.7. Apoptosis

A number of FDA approved anticancer agents induce cell killing through an apoptotic mechanism [56]. In a well-established dual-staining fluorescence-assisted cell-sorting (FACS) analysis that examines apoptosis, we observed a significant population of apoptotic cells in the early-to-late stages. The experiment takes advantage of the polarized cell membrane of cells undergoing apoptosis and, in the

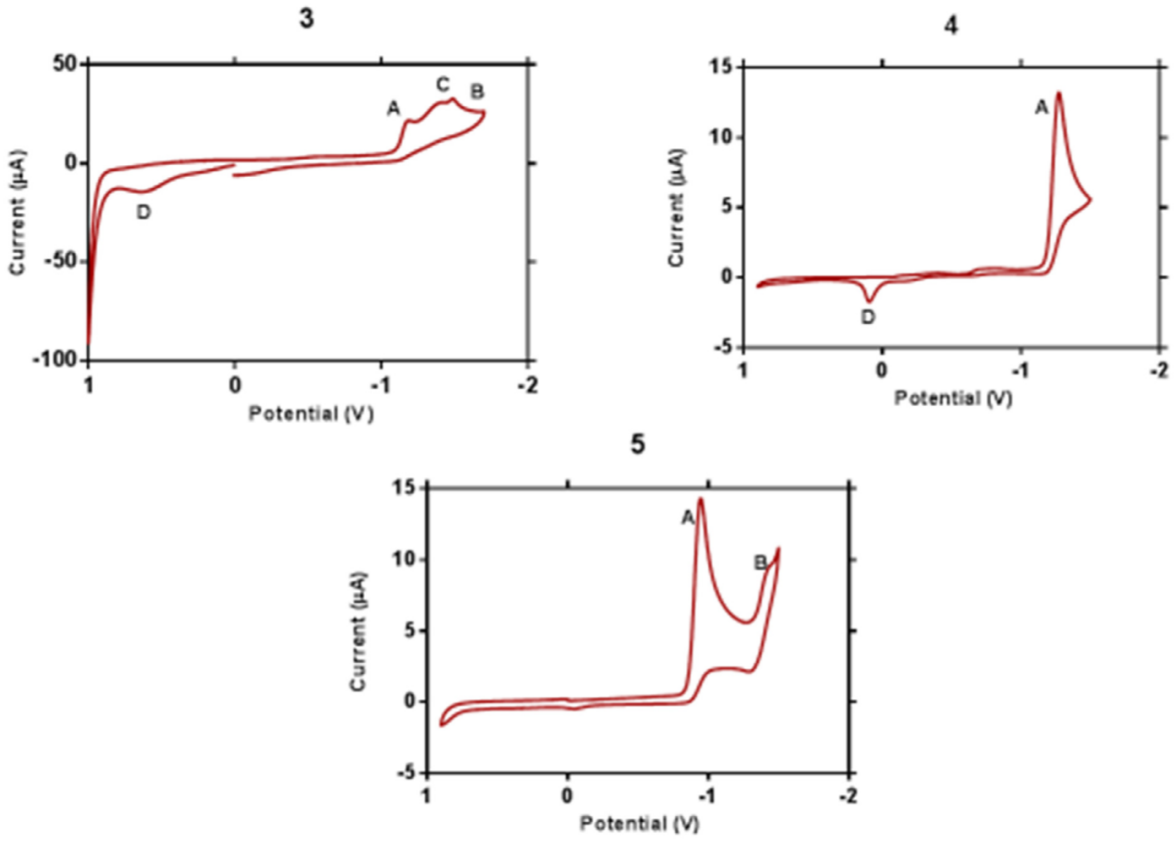

Fig. 3. Cyclic voltammogram of complexes **3**, **4**, and **5**. The experiment was conducted at room temperature in anhydrous DMSO with 0.1 M NBu_4PF_6 electrolyte at a scan rate of 100 mV/s. The potential is referenced to Ag/AgCl based on the position of the Fc/Fc + couple as an internal standard.

Table 2
Experimentally determined reduction and oxidation potentials of complexes **3** – **5.**

	Reduction Potential (V)				Oxidation Potential (V)
Complex	Std. E	E (A)	E (B)	E (C)	E (D)
$Ge^{IV/II}$	−1.37				
$Ge^{II/0}$	−1.07				
3		−1.2	−1.9		0.65
4		−1.3			0.100
5		−0.9	−1.9		

process, expose phosphatidylserine that is recognized by FITC labeled Annexin V. A2780 cells were treated with **3** at different concentrations (5 or 10 μM) for 48 h (Fig. 6). This further confirms the bioactive property of Ge(IV)-β-diketonates and their utility in cancer treatment.

2.8. Cell cycle

We determined the effect of compound **3** on the cell cycle in A2780 cells by flow cytometry analysis using propidium iodide staining. As summarized in the bar graph of Fig. 7, incubation of **3** at 5 μM over a period of 72 h led to G1 arrest. The G1 arrest increased over time, from 70.00 ± 3.45% at 24 h to 82.94 ± 3.89% at 72 h, indicative of a potentially different mechanism of action from cisplatin, which induces G2/M arrest under similar conditions in A2780 cells [57]. Compounds that modulate the cell cycle for therapeutic gain is highly sought after since they could be used in targeted cancer therapy. A number of small-molecules that induce G1 arrest are in clinical trials and show remarkable promise. These compounds inhibit cyclin-dependent kinases, which are regulators of the cell cycle, specifically the G1 phase. Our studies show that Ge(IV) complexes induce G1 arrest and can benefit cancer treatment in a targeted fashion. A more detailed cell-cycle study is needed to identify the mechanism of the dominant cell-cycle arrest observed.

2.9. Mitochondria membrane potential

Biological processes that are often exploited by cytotoxic agents include mitochondria destabilization.[58] For a number of cancer types, targeting mitochondria dysfunction can be an effective methodology for improving cancer treatments [58–60]. The mitochondria membrane potential (Δm) is the critical driving force for mitochondrial ATP synthesis and its depolarization often result in altered mitochondrial function, which could be useful or detrimental to cell state [61–64]. Therefore, we studied the mitochondrial function of A2780 cells in the presence or absence of complex **3** using fluorescence microscopy. Following the incubation of A2780 cells with **3** at 10 μM for 4 h, cells were then exposed to JC-1 dye and subsequently probed using confocal microscopy. We observed that **3** induced depolarization in cells, evidenced by the increase in green fluorescence (J-monomers) in contrast to the red fluorescence (J-aggregates) from untreated cells [65]. The uncoupler, CCCP was used as control by treating cells with 100 μM for 1 h. Under the condition, very few J-aggregates were observed in comparison to that of **3** (Fig. 8). Taken together, **3** evokes mitochondria membrane depolarization that may be the likely culprit for apoptosis induction.

2.10. ROS accumulation

Consequently, we examined the potential for **3** to generate

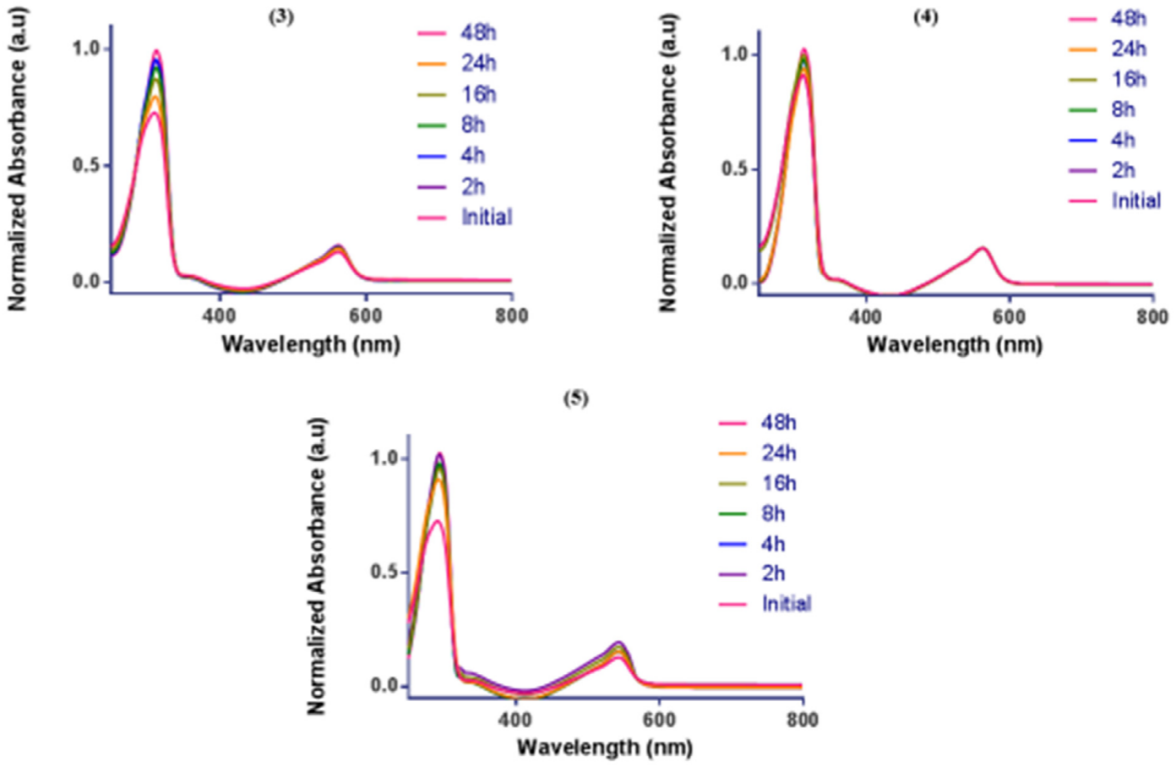

Fig. 4. UV–vis studies of complexes **3**, **4**, and **5**. The experiment was conducted at room temperature in DMEM media to mimic biological conditions. Complexes were prepared as a stock solution in DMSO and diluted down to 50 μM in DMEM. The absorbances were taken at the annotated time intervals to determine complex stability.

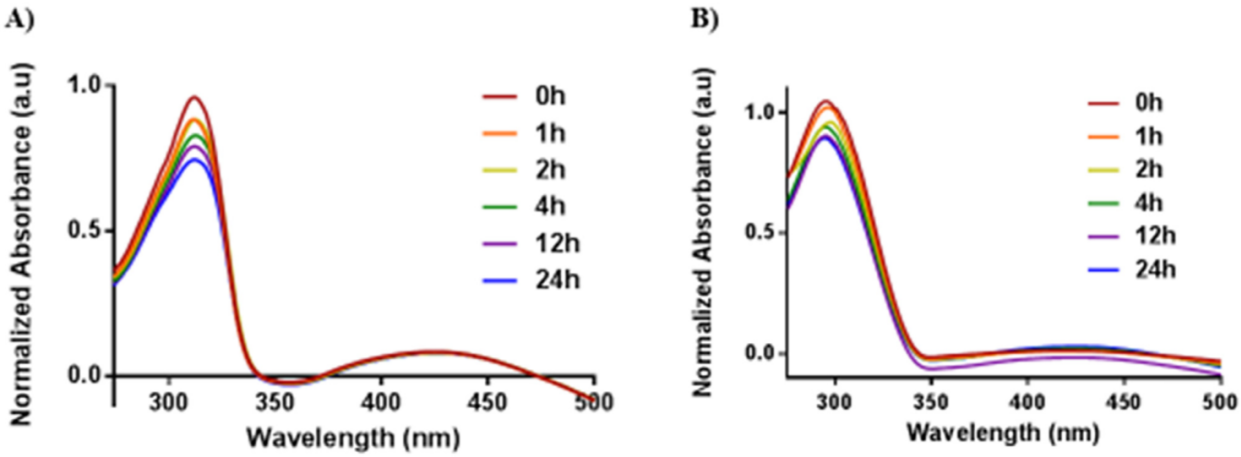

Fig. 5. A) UV–vis study of complex **3** (50 μM) with GSH (5 mM) in DMEM over 24 h. **B)** UV–vis study of complex **3** (50 μM) with NAC (5 mM) in DMEM over 24 h.

Table 3
In vitro cytotoxicity of complexes in cancer cells and the normal cell line, MRC5 using MTT assay. IC_{50}(μM) values obtained are an extrapolation from corresponding dose–response curves performed in triplicate and normalized to an untreated control. DMSO Stock solution of compounds used were serially diluted and added to cells with final DMSO concentration of < 1%.

Complex	IC_{50} (μM)				
	A2780	MDA-MB-231	MDA-MB-175	H460	MRC5
3	11.22 ± 0.33	10.42 ± 0.22	15.3 ± 0.25	13.3 ± 0.67	33.1 ± 2.12
4	9.15 ± 0.14	9.44 ± 0.82	15.7 ± 0.30	9.69 ± 0.42	38.0 ± 1.27
5	9.23 ± 0.33	10.9 ± 0.28	12.0 ± 0.26	11.5 ± 0.37	37.2 ± 1.64
Cisplatin	5.59[53]	36.2[53]	180[53]	4.7[54]	9.5[55]

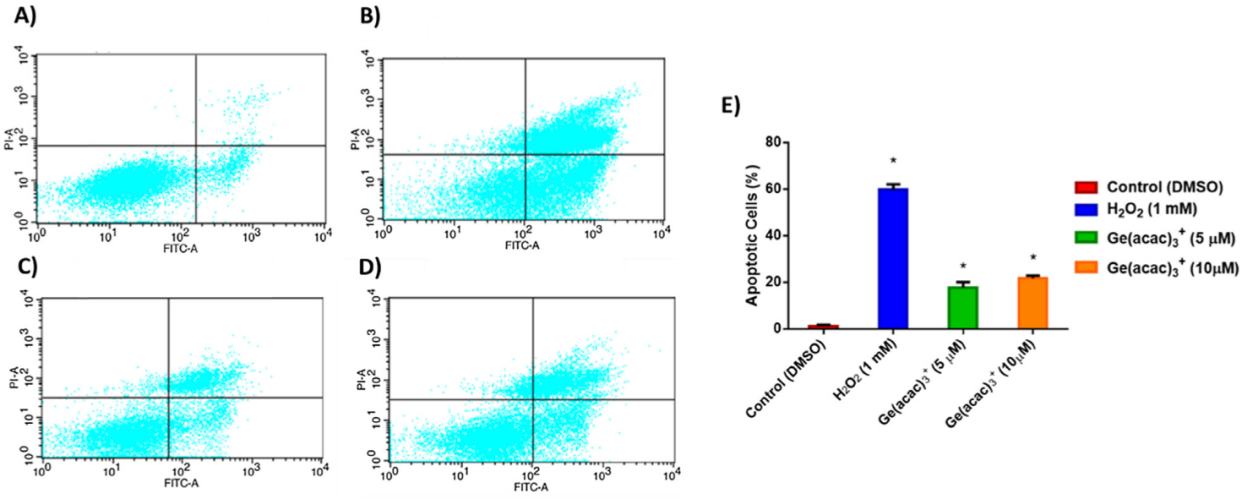

Fig. 6. Compound **3** induces apoptosis in A2780 cells. Cells were seeded at a density of 5×10^5. A) DMSO (48 h), B) H_2O_2 (2 mM for 3 h), C); **3** (5 μM for 48 h), D) **3** (10 μM for 48 h), graphs are representative of three individual experiments. E) Apoptotic cell percentages after treatment with compound and H_2O_2. Data are plotted as the mean ± s.e.m., * $P < 0.005$.

intracellular ROS as several apoptosis-inducing agents have the capacity to disrupt redox homeostasis by generating ROS or RNS. Using a cellular ROS assay, which uses the cell permeant reagent, 2′,7-dichlorofluorescein diacetate (DCF-DA), a fluorogenic dye capable of measuring hydroxyl, peroxyl and other ROS intracellularly via oxidation, following the deacetylation by cellular esterases to generate a highly fluorescent compound that can be detected by flow cytometry [66]. In this experiment A2780 cells treated with complex **3** for 1 h, displayed enhanced fluorescence than untreated cells by a factor of three, extrapolated from Fig. 9.

In support of ROS generation by **3**, we used the ROS inhibitor *N*-acetyl cysteine (NAC) to examine possible attenuation of complex **3** induced ROS. We found that when A2780 cells are pre-incubated with 10 mM of NAC, the fluorescence signal remains unchanged in comparison to the untreated control. This suggests that ROS are produced by the action of **3** in cells, which can be inhibited by NAC.

3. Conclusions

We have established the use of high-valent Ge(IV)-diketonate as potential anticancer agents and investigated their mode of action. The synthesis of these compounds followed a streamlined protocol that used $GeCl_2$·dioxane and acetylacetone as starting materials. Complexes with different anions were synthesized from the mixed valence $[Ge(acac)_3][GeCl_3]$ complex to afford **4**, **5**, and **6**. We gained insight into the electrochemical behavior of these compounds using cyclic voltammetry. Overall, complex **4** with the SbF_6^- anion proved to be the most stable with no Ge(II)/Ge(0) reduction couple observed. This was corroborated by solution studies in DMEM, which showed an unaltered UV–vis profile over 48 h. The complexes demonstrate a dose-dependent anticancer activity in a panel of human cancer cell lines as well as significant apoptosis induction in ovarian A2780 cells. There was no significant difference in anionic effects on anticancer activity. To study the mode of action of the Ge(IV) compounds, cell-cycle studies in A2780 revealed a G1 arrest, which prompted us to investigate the ROS production induced by these compounds since the cell cycle pattern was differentiated from cisplatin, which induces G2/M – S phase arrest due to the formation of DNA cross links. Our compounds cause ROS accumulation and induce mitochondria membrane depolarization in cancer cells. This study makes the case for the development of Ge compounds

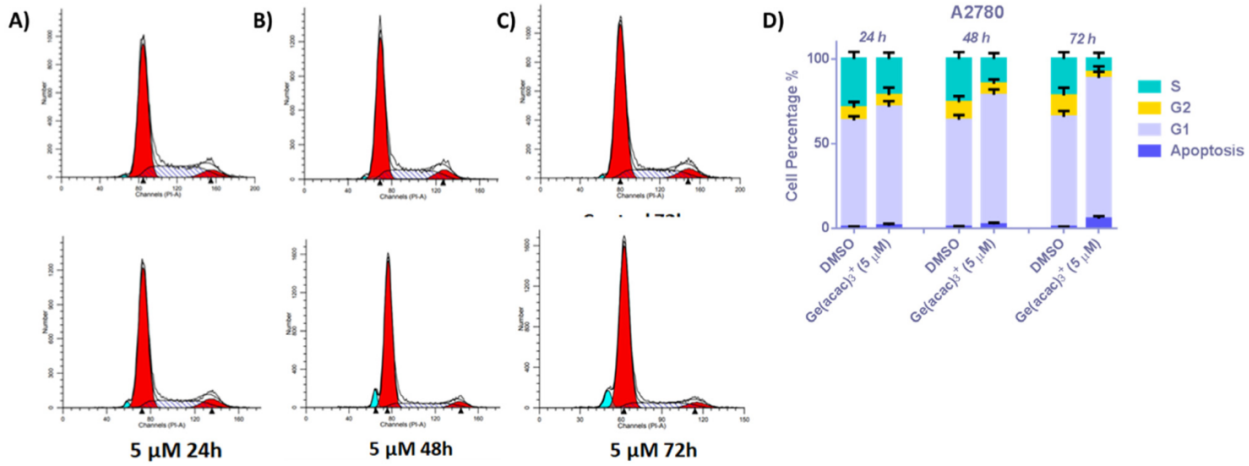

Fig. 7. Complex **3** induced G1 arrest in the cell cycle. Cells were seeded at a density of 5×10^5. Cells were treated for 24, 48, and 72 h at 5 μM. A) 24 h, Top: DMSO; bottom: treated cells. B) 48 h, Top: DMSO; bottom: treated cells. C) 72 h, Top: DMSO; bottom: treated cells. D) Representative S, G1, G2, and apoptotic cells percentages at time intervals 24, 48 and 72 h. Data are representative of triplicate experiments and plotted as plotted as the mean ± s.e.m.

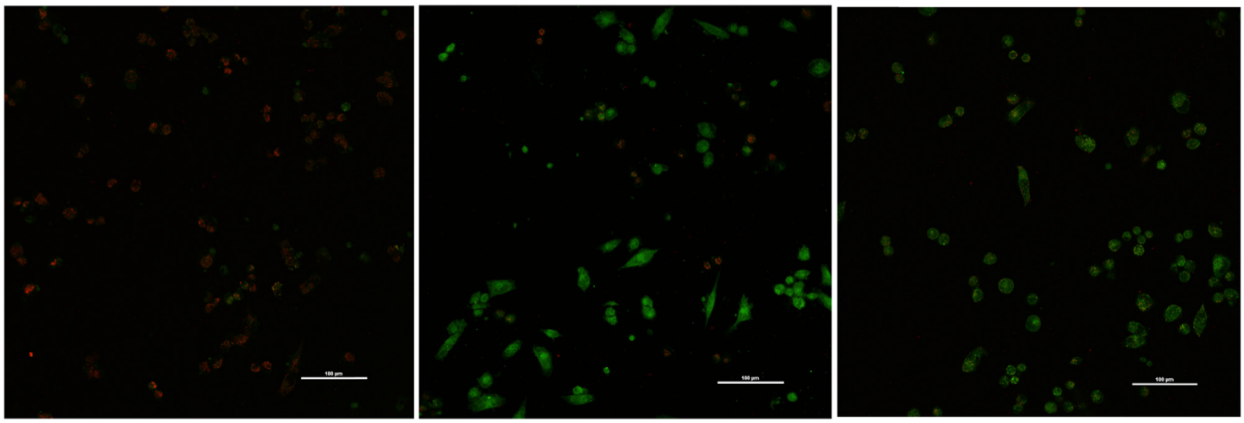

Fig. 8. Mitochondrial membrane potential (MMP) was visualized using confocal microscopy *via* JC-1. J-aggregates are shown in red (excitation/emission : 510/590 nm) and J-monomers in green (excitation/emission : 488/525 nm). Shown above left to right (DMSO, **3** 10 μM for 4 h, and CCCP 100 μM for 1 h). (For interpretation of the references to colour in this figure legend, the reader is referred to the web version of this article.)

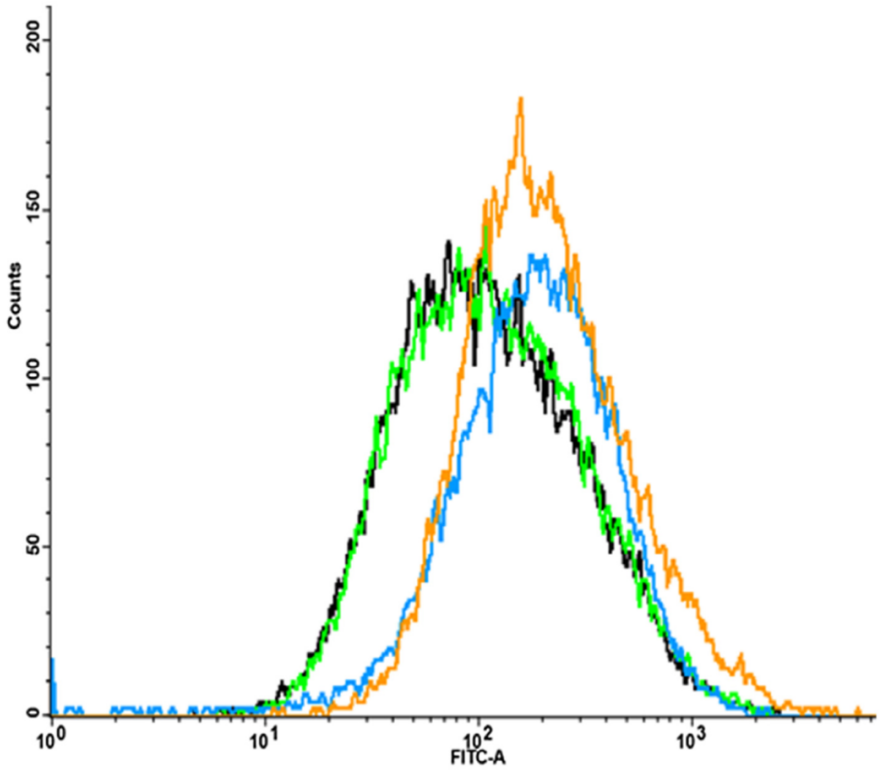

Fig. 9. DCF-DA ROS accumulation was monitored using FACS FITC-A channel (exc. 488 nm). Cells were seeded at a density of 5×10^5 cells. (Black) DMSO control, (Green) NAC pre-treatment for 2 h at 10 mM followed by treatment with **3** at 10 μM for 1 h, (Orange) treatment with **3** at 10 μM for 1 h, (Blue) treatment with H_2O_2 at **3** mM for 1 h. The curves shown are representative of three independent experiments. (For interpretation of the references to colour in this figure legend, the reader is referred to the web version of this article.)

as anticancer agents.

4. Experimental section

4.1. Chemistry

4.1.1. Experimental

4.1.1.1. General experimental and materials. All reactions and manipulations were carried out under normal atmospheric conditions unless otherwise stated. $GeCl_2$·Dioxane was purchased from Strem Chemicals. Acetylacetone was purchased from Sigma Aldrich and used as received. L-glutathione and *N*-acetyl cysteine were purchased from Alfa Aesar. All other solvents were of ACS grade and used as commercially available. Deuterated solvents were purchased from Cambridge Isotope Laboratories (Andover, MA). 3-(4,5-dimethylthiazol-2-yl)-2,5-diphenyltetrazolium bromide (MTT) and 2′,7′ –dichlorofluorescin diacetate (DCF-DA), and JC-1 were purchased from Cayman Chemicals. We utilized ACS grade solvents, which were purchased from Pharmco-Aaper and used without further purification or drying. Deuterated solvents were purchased from Cambridge Isotope Laboratories and used as received. Silica gel for column chromatography (Silicycle, P/N: R10030B SiliaFlash®F60, Size: 40–63 μm, Canada) was purchased from Silicycle. Aluminum backed silica-gel plates (20×20 cm^2) were purchased from Silicycle (TLA-R10011B-323) and utilized for analytical thin-layer chromatography (TLC). Filtrations were carried out using medium-porosity ceramic funnels. Removal of solvents in vacuo was performed using a Büchi rotary evaporator and further drying was achieved by Schlenk line at ~120 mTorr using a dynamic vacuum pump.

4.1.1.2. Physical measurements. ^{1}H NMR ^{13}C NMR, and ^{19}F NMR spectra were recorded at 400, 101, and 376 MHz on a Bruker Avance NEO spectrometer at the University of Kentucky NMR Center. Chemical shifts were internally referenced to solvent signals; (^{1}H NMR DMSO-d_6 at δ = 2.50 ppm, ^{13}C NMR DMSO-d_6 at δ = 39.52 ppm) and externally referenced to $CFCl_3$ δ = 0.00 ppm for ^{19}F NMR. Elemental analysis for C and H was performed at Atlantic Microlabs, Inc. (Norcross, GA) with a combustion temperature of 1400 °C.

Liquid chromatography mass spectra (LC-MS) were obtained using an Agilent 1200 HPLC with a a direct flow injection with a HPLC auto sampler without a column (injection volume: 40 μL, flow rate: 0.2 mL/min). ESI positive mode was taken with a source temperature of 120 °C, desolvation temperature of 300 °C, Capillary Vat 3.5 kV while Cone was set at 35.

In addition to spectroscopic characterization, the purity of all compounds was assessed by RP-HPLC using an Agilent Technologies 1100 series HPLC instrument and an Agilent Phase Eclipse Plus C18 column (4.6 mm × 100 mm; 3.5 μm particle size). All compounds were found to be ≥ 97% pure.

4.1.1.3. Synthesis. Synthesis of compounds **3 – 5** were carried out at room temperature under ambient conditions. Synthesis of complex **6** was performed under a stream of N_2. Compounds **3 – 5** were isolated as white solids and are benchtop stable at room temperature. They are soluble in MeCN, MeOH, DMF, and DMSO. They are slightly soluble in acetone and not soluble in Et_2O, hexanes, and pentane. Full synthetic procedures and complete characterization can be found in the supporting information.

4.1.1.4. UV-vis spectrometry. All spectra were recorded on a Shimadzu UV-vis 1280 spectrophotometer. Compounds were prepared as a stock in DMSO prior to dilution into DMEM. DMEM was warmed to room temperature prior to use. The DMEM was not supplemented with penicillin, streptomycin, or fetal bovine serum (FBS).

4.1.1.5. X-ray crystallography. Crystals of **3–5** were grown from slow diffusion of Et_2O into a concentrated MeCN solution. Crystals of **6** were grown from slow evaporation of a THF solution on a Schlenk line. All crystals were mounted using polyisobutene oil onto the tip of a glass fibre under a cool stream of nitrogen gas [67,68]. Diffraction data were collected by using Mo Kα radiation (0.71073 Å) using a Bruker D8 Venture diffractometer. Raw data were integrated, scaled and merged using the APEX3 package [69–71]. Determination of the space group and structure solution were carried out using SHELXT [72]. Structure refinement was performed using SHELXL [73]. All non-hydrogen atoms were refined using anisotropic displacement parameters. Ellipsoid plots were drawn using SHELXTL-XP [73].

4.2. Biological methods and materials

4.2.1. Cell lines and culture

All cell lines used MDA-MB-231 and MDA-MB-175 (triple negative breast cancer), A2780 (ovarian adenocarcinoma), and H460 (non-small-cell lung cancer were purchased from ATCC and routinely grown in a humidified incubator at 37 °C with 5–10% CO_2. Culture media and supplements were purchased from Corning Inc. MDA-MD-175, MDA-MB-231, MRC5, H460 were grown using Dulbecco's Modified Eagle Medium (DMEM) was supplemented with 10% FBS, and 1% Penicillin/streptomycin. A2780 were grown using Roswell Park Memorial Institute 1640 (RPMI 1640) supplemented with 10% FBS, 1% Penicillin/streptomycin, 4 mM and glutamine.

4.2.2. UV-vis stability

Compounds **3–6** were prepared as a 5 mM stock in DMSO and diluted to a final concentration of 50 μM in DMEM with no supplements added. The UV–vis absorbance profile was taken at different time intervals over a period of 48 h to monitor stability in solution. Prior to each run, the absorbance baseline was properly adjusted with a fresh DMEM solution.

4.2.3. Reactivity with L-Glutathione (GSH) and N-Acetyl cysteine (NAC)

The DMEM used was supplemented with 10% FBS, 1% Penicillin/streptomycin and was used to bank the instrument prior to each experiment. Compound **3** was prepared as a 10 mM stock in DMSO and diluted to 100 μM (4 mL) with DMEM. GSH and NAC were prepared as 10 mM stock solutions in DMEM. For each respective experiment, 2 mL of the 100 μM stock of **3** was added to 2 mL of the 10 mM stock of either GSH or NAC and mixed thoroughly to achieve a homogenous solution of **3** (50 μM) and GSH/NAC (5 mM). The first scan was taken and recorded as 0 h. All subsequent scans were recorded at their respective time intervals. Data were normalized with Excel with respect to the run titled 0 h and plotted in GraphPad Prism 6.

4.2.4. Cell viability assay using MTT

The various cell lines were seeded on a clear bottomed 96 well plate at a density of 2,000 cells/well and incubated in the appropriate media overnight. Stock solutions of complexes **3–5** were prepared in DMSO and added to the wells, not exceeding 1% DMSO into the well. Cells were treated for 72 h at 37 °C. The media was removed and replaced and added 100 μL of MTT solution (prepared by making 5 mg/mL solution of MTT in PBS and diluting 10x with the appropriate media). The cells were incubated at 37 °C for 4 h with the MTT dye. The dye was then removed and added 100 μL of DMSO to induce cell lysis. The plates were read sing a Genios plate reader (570 nm). All experiments were performed in triplicates.

4.2.5. Apoptosis analysis

A780 cells were seeded in 6 well plates at a density of 5x10^5 cells/well and allowed to adhere overnight at 37 °C. Cells were treated with different concentrations (5 and 10 μM) for 48 h·H_2O_2 was used as a positive control (2 mM for 3 h). Staining of apoptotic cells was done using Annexin V-FITC, Annexin V-PI (propidium iodide) and and Annexin binding buffer as per the manufacturer's instructions. Cells were sorted using fluorescence-activated cell sorting (FACS) analysis. All experiments were performed in triplicate. Data was plotted using the FloJo software.

4.2.6. Cell cycle analysis

A2780 cells were seeded in 6 well plates at a density of 5 × 10^5 cells/well and allowed to adhere overnight at 37 °C. Cells were treated at a fixed concentration (5 μM) and treated for time periods of 24, 48, and 72 h. After the treatment condition, cells were harvested via trypsinization and pelleted. The collected pellets were washed twice with PBS (1 mL) and incubated at 4 °C with RNAse solution (50 μL of 100 μg/mL) for 20 min. Then 200 μL of PI (50 μg/mL) and the solution filtered through a cell strainer cap (VWR) into a 5 mL Coning Falcon test tube. The samples were analyzed using FACS. All experiments were performed in triplicate. Data was plotted using the FloJo software.

4.2.7. Intracellular ROS accumulation assay

A2780 cells were seeded at a density of 5 × 10^5 cells/well in 6 well plates and allowed to adhere overnight at 37 °C. Cells were treated at a fixed concentration of (10 μM) for 1 h·H_2O_2 (500 μM) for 1 h was used a positive control. For samples with *N*-acetyl cysteine (NAC) treatment, cells were treated with a 10 mM stock of NAC in PBS 2 h prior before addition of the compound. After treatment, the cells were washed with PBS (2 × 2 mL) and collected via trypsinization. The cells were pelleted and resuspended in 0.5 mL of a DCF-DA (10 μM) solution in PBS. The cells were centrifuged again and resuspended in PBS. The cells were analyzed using FACS; FITC (488 nm) channel. All experiments were run in triplicate. The data were plotted with FloJo.

4.2.8. Mitochondrial membrane potential assay

A2780 cells were seeded at a density of 2 × 10^5 cells in a glass bottom dish with a #1.5 mm glass cover slip (VWR). Cells were allowed to adhere overnight at 37 °C. Cells were treated at a fixed concentration (10 μM) for 4 h. Carbonyl cyanide m-chlorophenyl hydrazine (CCCP), a known OXPHOS inhibitor, was used as a positive control (100 μM, 1 h). After treatment, cells were washed with PBS (2 × 3 mL). JC-1 dye solution was prepared from the purchased kit according to the manufacturer's instructions (Cayman Chemicals). In short, 100 μL of stock solution was diluted x10 in phenol red free media to prepare the working solution. Per every 1 mL of culture media, 100 μL of working solution was added and the cells incubated at 37 °C for 30 min. The media was removed and added 2 mL of PBS and the samples placed on ice. The cells were imaged with a Nikon A1R Inverted Confocal Microscope. J-aggregates were imaged with (excitation/emission: 510/590 nm) and J-monomers with (excitation/emission: 488/525 nm).

4.2.9. Data processing

All biological data were plotted using GraphPad Prism 6 unless otherwise noted. Statistical analysis was performed using GraphPad Prism 6. Images were processed with NIS-Elements software.

4.2.10. Electrochemistry

Complexes **3–5** were prepared as a 5.0 mM stock solution in DMSO. NBu_4PF_6 (0.1 mM) was used as the electrolyte in DMSO for all runs. All electrochemical measurements were performed at room temperature by using CH instruments 650E potentiostat, which contains three electrodes, each 3 mm diameter glassy-carbon working electrode, platinum wire counter electrode, and a Ag/AgCl reference electrode.

4.3. Accession codes

CCDC 1964207, 1964208, 1964209, 1,964,210 contain the supplementary crystallographic data for this paper. These data can be obtained free of charge via www.ccdc.cam.ac.uk/data_request/cif, by emailing data_request@ccdc.cam.ac.uk, or by contacting The Cambridge Crystallographic Data Centre, 12, Union Road, Cambridge CB2 1EZ, UK; fax: +44 1223 336033.

CRediT authorship contribution statement

Randall T. Mertens: Conceptualization, Methodology, Validation, Writing - original draft, Investigation, Formal analysis. **Sean Parkin:** Data curation. **Samuel G. Awuah:** Supervision, Funding acquisition, Resources, Conceptualization, Methodology, Validation, Writing - original draft.

Declaration of Competing Interest

The authors declare that they have no known competing financial interests or personal relationships that could have appeared to influence the work reported in this paper.

Acknowledgements

We thank the University of Kentucky for start-up funding. We are very grateful for the facilities and staff at the University of Kentucky who supported the work presented in this manuscript. We would like to thank the UK NMR Center supported by NSF (CHE-997738) and the UK X-ray facility supported by the MRI program from NSF (CHE-1625732). We would like to also thank Greg Bauman Ph.D (UK Flow Cytometry and Immune Function core supported by the Office of the Vice President of Research, the Markey Cancer Center, and NCI Center Core Support Grant (P30 CA177558) as well as Thomas Wilkop Ph.D and Mr. James Schwartz (UK Light Microscopy Core) for their assistance. We are grateful for the use of Dr. Steven Van Lanen's laboratory (UK College of Pharmacy) for the use of their LC-MS. Elemental analysis was performed with the help of Atlantic Microlabs, Inc (Atlanta, Georgia).

Appendix A. Supplementary data

Supplementary data to this article can be found online at https://doi.org/10.1016/j.ica.2019.119375.

References

[1] R.L. Siegel, K.D. Miller, A. Jemal, CA Cancer J. Clin. 69 (2019) 7–34.
[2] V. Mathews, B. George, E. Chendamarai, K.M. Lakshmi, S. Desire, P. Balasubramanian, A. Viswabandya, R. Thirugnanam, A. Abraham, R.V. Shaji, A. Srivastava, M. Chandy, J. Clin. Oncol. 28 (2010) 3866–3871.
[3] Z.-Y. Wang, Z. Chen, Blood 111 (2008) 2505–2515.
[4] K.D. Mjos, C. Orvig, Chem. Rev. 114 (2014) 4540–4563.
[5] S. Dasari, P. Bernard Tchounwou, Eur. J. Pharmacol. 740 (2014) 364–378.
[6] B. Lippert, Cisplatin: chemistry and biochemistry of a leading anticancer drug, Zürich : Verlag Helv. Chim. Acta, Weinheim New York : Wiley-VCH, Zürich : Weinheim New York, 1999.
[7] F.M. Muggia, A. Bonetti, J. Hoeschele, M. Rozencweig, S.B. Howell, J. Clin. Oncol. 35 (2015) 4219–4226.
[8] S.R. McWhinney, R.M. Goldberg, H.L. McLeod, Mol. Cancer Ther. 8 (2009) 10–16.
[9] A. Field-Smith, G.J. Morgan, F.E. Davies, Ther. Clin. Risk Manag. 2 (2006) 271–279.
[10] V. Mathews, B. George, K.M. Lakshmi, A. Viswabandya, A. Bajel, P. Balasubramanian, R.V. Shaji, V.M. Srivastava, A. Srivastava, M. Chandy, Blood 107 (2006) 2627–2632.
[11] E. Lengfelder, W.K. Hofmann, D. Nowak, Leukemia 26 (2012) 433–442.
[12] A.K. Haldar, P. Sen, S. Roy, Mol. Bio. Int. 2011 (2011) 23.
[13] J. Pi, J. Zeng, J.-J. Luo, P.-H. Yang, J.-Y. Cai, Bioorg. Med. Chem. Lett. 23 (2013) 2902–2908.
[14] P.W. Kaplan BJ, Andrus GM, Simpson JS, Field CJ., J. Altern. Complement. Med., 10 (2004) 337-344.
[15] S.L. Jiang, C.H. Shi, J.G. Wu, J. Food Chem. 30 (2007) 481–495.
[16] O. Wiche, V. Zertani, W. Hentschel, R. Achtziger, P. Midula, J. Geochem. Explor. 175 (2017) 120–129.
[17] A.F. Koca, I. Koca, B. Tekguler, Acta Hortic. 1143 (2016) 297–302.
[18] E. Kim, S.-U. Hwang, J.D. Yoon, E.-B. Jeung, E. Lee, D.Y. Kim, S.-H. Hyun, J. Reprod. Dev. 63 (2017) 581–590.
[19] T. Wada, T. Hanyu, K. Nozaki, K. Kataoka, T. Kawatani, T. Asahi, N. Sawamura, Bio. Pharm. Bull. 41 (2018) 749–753.
[20] D.D. Vaughn Ii, R.E. Schaak, Chem. Soc. Rev. 42 (2013) 2861–2879.
[21] S.-J. Chiu, M.-Y. Lee, W.-G. Chou, L.-Y. Lin, Radiat. Res. 159 (2003) 391–400.
[22] M.-H. Lin, T.-S. Hsu, P.-M. Yang, M.-Y. Tsai, T.-P. Perng, L.-Y. Lin, Int. J. Radiat. Biol. 85 (2009) 214–226.
[23] X.-Y. Su, P.-D. Liu, H. Wu, N. Gu, Cancer Biol. Med. 11 (2014) 86–91.
[24] A.M. Badger, C.K. Mirabelli, M. DiMartino, Int. Immunopharmacol. 10 (1985) 201–207.
[25] S.S. Legha, J.A. Ajani, G.P. Bodey, J. Clin. Oncol. 1 (1983) 331–336.
[26] D.S. Ettinger, D.M. Finkelstein, R.C. Donehower, A.Y.C. Chang, M. Green, R. Blum, R.G. Hahn, J.C. Ruckdeschel, Med. Pediatr. Oncol. 17 (1989) 197–201.
[27] D.S. Ettinger, D.M. Finkelstein, M.D. Abeloff, Y.C. Chang, T.J. Smith, M.M. Oken, J.C. Ruckdeschel, Invest. New Drugs 8 (1990) 183.
[28] Y. Nakamura, K. Isobe, H. Morita, S. Yamazaki, S. Kawaguchi, Inorg. Chem. 11 (1972) 1573–1578.
[29] G.M. Bancroft, A.G. Maddock, W.K. Ong, R.H. Prince, J. Chem. Soc. A. (1966) 723–725.
[30] M. Cox, R.J.H. Clark, H.J. Milledge, Nature 212 (1966) 1357–1357.
[31] J.E. Collins, M.P. Castellani, A.L. Rheingold, E.J. Miller, W.E. Geiger, A.L. Rieger, P.H. Rieger, Organometallics 14 (1995) 1232–1238.
[32] A. Muscella, N. Calabriso, C. Vetrugno, F.P. Fanizzi, S.A. De Pascali, C. Storelli, S. Marsigliante, Biochem. Pharmacol. 81 (2011) 91–103.
[33] C. Garand, D. Guay, C. Sereduk, D. Chow, S.P. Tsofack, M. Langlois, È. Perreault, H.H. Yin, M. Lebel, Cancer Sci. 102 (2011) 1410–1417.
[34] G.T. Morgan, A.R. Bowen, J. Chem. Soc., Trans. 125 (1924) 1252–1261.
[35] W.K. Ong, R.H. Prince, J. Inorg. Nucl. Chem. 27 (1965) 1037–1042.
[36] J.P.M. Ralph, C. Young, Inorg. Synth. McGraw-Hill Book Company, Inc., 1946, pp. 25–26.
[37] A. Forman, L.E. Orgel, Mol. Phys. 2 (1959) 362–366.
[38] G.S. Smith, P.B. Isaacs, Acta Cryst. 17 (1964) 842–846.
[39] K.M. Baines, W.G. Stibbs, Coord. Chem. Rev. 145 (1995) 157–200.
[40] C. Glidewell, D.C. Liles, J. Organomet. Chem. 174 (1979) 275–279.
[41] B. Morosin, L.A. Harrah, Acta Crystallogr. Sect. B 37 (1981) 579–586.
[42] S. Masamune, S.A. Batcheller, J. Park, W.M. Davis Acta Crystallogr. Sect. B, O. Yamashita, Y. Ohta, Y. Kabe, J. Am. Chem. Soc., 111, 1989, 1888–1889.
[43] NIST Computational Chemistry Comparison and Benchmark Database, N.S.R.D.N. 101, A. Release 20, Editor: Russell D. Johnson III, http://cccbdb.nist.gov/.
[44] P.N. Bartlett, C.Y. Cummings, W. Levason, D. Pugh, G. Reid, Chem. Eur. J. 20 (2014) 5019–5027.
[45] M.R.M. Williams, B. Bertrand, D.L. Hughes, Z.A.E. Waller, C. Schmidt, I. Ott, M. O'Connell, M. Searcey, M. Bochmann, Metallomics 10 (2018) 1655–1666.
[46] G. Boscutti, L. Marchiò, L. Ronconi, D. Fregona, Chem. Eur. J. 19 (2013) 13428–13436.

[47] K.K. Starheim, T. Holien, K. Misund, I. Johansson, K.A. Baranowska, A.M. Sponaas, H. Hella, G. Buene, A. Waage, A. Sundan, G. Bjørkøy, Blood Cancer J., 6 (2016) e446-e446.
[48] A. Meister, J. Biol. Chem. 263 (1988) 17205–17208.
[49] M. Williams, A.I. Green, J. Fernandez-Cestau, D.L. Hughes, M.A. O'Connell, M. Searcey, B. Bertrand, M. Bochmann, Dalton Trans. 46 (2017) 13397–13408.
[50] F. Meriggi, B. Di Biasi, A. Zaniboni, J. Chemotherapy 20 (2008) 551–560.
[51] N.C. Turner, A.N.J. Tutt, Breast Cancer Res. 14 (2012) 115.
[52] J. Jin, W. Zhang, W. Ji, F. Yang, X. Guan, Cancer Biol. Ther. 18 (2017) 369–378.
[53] M.G.H.C.C. Cancer Genome Project at the Wellcome Sanger Institute and Center for Molecular Therapeutics, in, Wellcome Sanger Institute, 2019.
[54] C.A. Rabik, M.L. Fishel, J.L. Holleran, K. Kasza, M.R. Kelley, M.J. Egorin, M.E. Dolan, J. Pharmacol. Exp. Ther. 327 (2008) 442–452.
[55] S. Dhar, S.J. Lippard, PNAS 106 (2009) 22199–22204.
[56] D. Green, G. Kroemer, J. Clin. Inestig. 115 (2005) 2610–2617.
[57] V. Pichler, S. Göschl, E. Schreiber-Brynzak, M.A. Jakupec, M. Galanski, B.K. Keppler, Metallomics 7 (2015) 1078–1090.
[58] D.R. Green, J.C. Reed, Science 281 (1998) 1309–1312.
[59] G. Battogtokh, Y.S. Choi, D.S. Kang, S.J. Park, M.S. Shim, K.M. Huh, Y.-Y. Cho, J.Y. Lee, H.S. Lee, H.C. Kang, Acta Pharm. Sin. B. 8 (2018) 862–880.
[60] P.E. Porporato, N. Filigheddu, J.M.B.-S. Pedro, G. Kroemer, L. Galluzzi, Cell Res. 28 (2018) 265–280.
[61] L. Galluzzi, N. Larochette, N. Zamzami, G. Kroemer, Oncogene 25 (2006) 4812–4830.
[62] L.D. Zorova, V.A. Popkov, E.Y. Plotnikov, D.N. Silachev, I.B. Pevzner, S.S. Jankauskas, V.A. Babenko, S.D. Zorov, A.V. Balakireva, M. Juhaszova, S.J. Sollott, D.B. Zorov, Anal. Biochem. 552 (2018) 50–59.
[63] H. Pelicano, W. Zhang, J. Liu, N. Hammoudi, J. Dai, R.-H. Xu, L. Pusztai, P. Huang, Breast Cancer Res. 16 (2014) 434.
[64] S. NavaneethaKrishnan, J.L. Rosales, K.-Y. Lee, Oncogene 37 (2018) 1788–1804.
[65] A. Perelman, C. Wachtel, M. Cohen, S. Haupt, H. Shapiro, A. Tzur, Cell Death Dis. 3 (2012).
[66] K.S. Eruslanov E., Armstrong D. Advanced Protocols in Oxidative Stress II. Methods in Molecular Biology, 594, 2010.
[67] S. Parkin, H. Hope, J. Appl. Cryst. 31 (1998) 945–953.
[68] H. Hope, Progress in Inorg. Chem. 41 (41) (1994) 1–19.
[69] Bruker, "APEX2" Bruker-AXS, Madison, WI. USA, 2006.
[70] L. Krause, R. Herbst-Irmer, G.M. Sheldrick, D. Stalke, J. Appl. Cryst. 48 (2015) 3–10.
[71] G.M. Sheldrick, SADABS, Program for bruker area detector absorption correction., University of Gottingen, Gottingen, 1997.
[72] G.M. Sheldrick, Acta Cryst. Sec. A. 71 (2015) 3–8.
[73] G. Sheldrick, Acta Cryst. Sec. A. 64 (2008) 112–122.